Free Radical Research, December 2014; 48(12): 1494–1504

ISSN 1071-5762 print/ISSN 1029-2470 online
DOI: 10.3109/10715762.2014.966706

informa
healthcare

ORIGINAL ARTICLE

Oxidative stress and susceptibility to mitochondrial permeability transition precedes the onset of diabetes in autoimmune non-obese diabetic mice

C. Malaguti[1], P. G. La Guardia[1†], A. C. R. Leite[1,2], D. N. Oliveira[1], R. L. de Lima Zollner[3], R. R. Catharino[1], A. E. Vercesi[1] & H. C. F. Oliveira[2]

[1]*Departamentos de Patologia Clínica, Universidade Estadual de Campinas, SP, Brasil,* [2]*Biologia Estrutural e Funcional, Universidade Estadual de Campinas, SP, Brasil, and* [3]*Clínica Médica, Universidade Estadual de Campinas, SP, Brasil*

Abstract

Beta cell destruction in type 1 diabetes (TID) is associated with cellular oxidative stress and mitochondrial pathway of cell death. The aim of this study was to determine whether oxidative stress and mitochondrial dysfunction are present in T1D model (non-obese diabetic mouse, NOD) and if they are related to the stages of disease development. NOD mice were studied at three stages: non-diabetic, pre-diabetic, and diabetic and compared with age-matched Balb/c mice. Mitochondria respiration rates measured at phosphorylating and resting states in liver and soleus biopsies and in isolated liver mitochondria were similar in NOD and Balb/c mice at the three disease stages. However, NOD liver mitochondria were more susceptible to calcium-induced mitochondrial permeability transition as determined by cyclosporine-A-sensitive swelling and by decreased calcium retention capacity in all three stages of diabetes development. Mitochondria H_2O_2 production rate was higher in non-diabetic, but unaltered in pre-diabetic and diabetic NOD mice. The global cell reactive oxygen species (ROS), but not specific mitochondria ROS production, was significantly increased in NOD lymphomononuclear and stem cells in all disease stages. In addition, marked elevated rates of 2',7'-dichlorodihydrofluorescein (H_2DCF) oxidation were observed in pancreatic islets from non-diabetic NOD mice. Using matrix-assisted laser desorption/ionization (MALDI) mass spectrometry (MS) and lipidomic approach, we identified oxidized lipid markers in NOD liver mitochondria for each disease stage, most of them being derivatives of diacylglycerols and phospholipids. These results suggest that the cellular oxidative stress precedes the establishment of diabetes and may be the cause of mitochondrial dysfunction that is involved in beta cell death.

Keywords: type 1 diabetes, mitochondria, reactive oxygen species, lymphomononuclear cells, pancreatic islet

Introduction

Type 1 diabetes (T1D) is an autoimmune disease initiated by inflammation (insulitis) caused by macrophages and T cells infiltration into the pancreatic islets followed by the release of pro-inflammatory cytokines and destruction of insulin-producing pancreatic β-cells. The destruction of β-cells in T1D is associated with oxidative and nitro-oxidative cellular stress [1,2]. An increase in the generation of reactive oxygen species (ROS) is probably mediated by inflammatory cytokines such as interleukin-1β (IL-1β), interferon-γ (IFN-γ), and tumor necrosis factor-α (TNF-α), which are produced by the activated T lymphocytes and are responsible for inducing dysfunction and death of β-cells [1,3,4]. The transduction of the signals that induce β-cells death can occur by different mechanisms that ultimately interfere with the activity of the Bcl-2 protein family, the mitochondrial membrane permeabilization, and the activity of caspases [5,6].

Mitochondria dysfunction has been implicated in the pathogenesis of metabolic diseases, mainly because it is an important source as well as target of ROS. In physiological conditions, mitochondria generate a small amount of superoxide radical at the level of respiratory complexes I and III. However, mitochondria have a powerful antioxidant system to detoxify excess of reactive oxygen production to prevent oxidative stress [7,8]. Excess of ROS production in the presence of increased intracellular Ca^{2+} concentration leads to mitochondrial permeability transition (MPT), a condition caused by the formation of a non-selective pore in the inner mitochondrial membrane that allows the release of cell death signaling molecules [9–11]. In addition to ROS, nitric oxide and nitrosothiols have emerged as important players in MPT regulation [12,13].

MPT is involved in many pathological processes, which encompass cellular Ca^{2+} overload and oxidative stress, for instance, ischemia–reperfusion [14]. We have previously reported that disturbances in lipid and glucose metabolism are associated with mitochondrial permeability transition [7,8,15–19]. Others have described MPT in cardiovascular diseases and obesity-related conditions [20,21].

The non-obese diabetic mouse model (NOD) was developed more than 30 years ago and provided advances in the understanding of the complex nature of autoimmune diseases [22,23]. The establishment of T1D in NOD mice is similar to what occurs in humans [24,25], beginning

[†]*in memorian*.

Correspondence: Helena C. F. Oliveira, Instituto de Biologia Universidade Estadual de Campinas, Unicamp, Cidade Universitária Zeferino Vaz, Rua Monteiro Lobato, 255 - Campinas, SP, Brasil, CEP 13083-862. Tel: + 55-19-35216204. E-mail: ho98@unicamp.br

(Received date: 18 June 2014; Accepted date: 12 September 2014; Published online: 14 October 2014)

with inflammatory cells infiltration into pancreatic cells followed by activation and release of inflammatory cytokines [26]. It is possible to study in NOD mice the different stages of the disease progress following the advancement of pancreatic β-cells destruction along with the loss of glycemic homeostasis [25,27].

Since β-cell destruction in T1D is associated with cellular oxidative stress and possibly with the mitochondrial pathway of cell death, the aim of this study was to determine whether oxidative stress and mitochondrial dysfunction are present in tissues of NOD mice and if they are related to the stages of the development of the disease. Considering the systemic inflammation of T1D and that the major triggers of inflammation (pro-inflammatory cytokines and chemokines) in islets can affect other tissues, we studied immune system cells as well as liver, muscle, and pancreatic islet. We determined mitochondria respiration, susceptibility to MPT and ROS production in liver and skeletal muscle biopsies, in isolated liver mitochondria, in spleen and circulating mononuclear cells, in bone marrow-derived hematopoietic stem cells, and in pancreatic islet from NOD mice, at different stages, before, during, and after the onset of diabetes.

Materials and methods

Animals

Female NOD/Unib mice and Balb/c were obtained from the Animal Breeding Center of the State University of Campinas (CEMIB/Unicamp, São Paulo, Brazil), under specific pathogen-free (SPF) conditions, and were maintained in an SPF animal facility at the Laboratory of Immunology (Faculty of Medical Sciences, Unicamp). The incidence of spontaneous diabetes in our colony is 85% in females up to 25 weeks of age (in non-manipulated mice). The animals were maintained under autoclaved water and food *ad libitum* and a light cycle of 12 hours. Mice were monitored for onset of diabetes by measurements of glucose concentration in blood obtained from the tail vein using glucose levels measured by a hand-held glucometer Optium™ (Abbott Diabetes Care Limited, United Kingston). The NOD mice were separated into three groups namely: 4–6 weeks old (non-diabetic, glycemia: <100 mg/dl), 7–10 weeks old (pre-diabetic, glycemia: 100–150 mg/dl), and 14–25 weeks old (diabetic glycemia: >250 mg/dl) as compared with age-matched control Balb/c mice. Experimental protocols were conducted according to the general guidelines established by The Brazilian College of Animal Experimentation (Cobea) and approved by the local Committee for Ethical in Animal Experimentation (protocol # 1335-1 CEUA/UNICAMP).

Isolation of liver mitochondria

Liver mitochondria from NOD/unib and Balb/c mice were isolated by conventional differential centrifugation [28]. Briefly, livers were homogenized in 250 mM of sucrose, 1 mM of ethylene glycol tetraacetic acid (EGTA), and 10 mM of Hepes buffer (pH 7.2), and centrifuged for 10 min at 2500 g. The supernatant was centrifuged for 10 min at 8000 rpm. The mitochondrial pellet was washed in medium containing 250 mM of sucrose, 10 mM of Hepes, and 0.1 mM of EGTA, and centrifuged for additional 10 min at 8000 g. The final pellet was resuspended in 250 mM of sucrose and 10 mM of Hepes to a final protein concentration of approximately 50–70 mg/ml. The experiments with isolated mitochondria were carried out at 28°C, with continuous magnetic stirring, in standard medium containing 125 mM of sucrose, 65 mM of KCl, 2 mM of inorganic phosphate, 1 mM of magnesium chloride, 10 mM of Hepes buffer (pH, 7.2), and a mixture of 5 mM of (nicotinamide adenine dinucleotide) NAD-linked substrates (malate + glutamate + ketoglutarate + pyruvate). Other additions are indicated in the figure legends.

Mitochondrial swelling

Mitochondrial swelling (0.5 mg/ml) was determined as the decrease in the turbidity of the mitochondrial suspension measured at 520 nm using a temperature-controlled Hitachi U-3000 spectrophotometer (28°C).

Mitochondrial calcium transport

Calcium uptake by isolated liver mitochondria (0.5 mg/ml) was determined following the fluorescence of 0.1 μM of Calcium Green-5N hexapotassium salt (Molecular Probes) using a temperature-controlled spectrofluorometer (Hitachi F4500, Tokyo, Japan) at 28°C, at excitation and emission wavelengths of 506 and 531 nm, respectively, and slit widths of 5.0 nm [29].

Islet isolation

The isolation of pancreatic islets was performed according to Ventura-Oliveira [27]. The pancreas was excised, minced, and digested with collagenase V (Sigma) for 24 min. Islets were isolated and collected under a dissection microscope with a micropipette.

Spleen mononuclear cells isolation

Spleen mononuclear cells were isolated with Histopaque 1077 (Sigma), as described before [30]. Cellular viability was tested using the trypan blue exclusion method, and it was considered satisfactory when the viability was over 95%.

Lymphomononuclear circulating cells isolation

The blood samples were collected in heparinized tubes for lymphomononuclear circulating cells isolation. The whole blood was layered on the Histopaque 1077 (Sigma) solution and centrifuged at 2000 g for 20 min. The lymphomononuclear cells are found at the interface between

plasma and Histopaque 1077. The supernatant was discarded and the cell fraction was resuspended in 5 ml of red cell lysis buffer, incubated for 15' at room temperature, and 5 ml of phosphate-buffered saline (PBS) was added to it and centrifuged at 1500 g for 10 min. The cells were washed once more with PBS at 1500 g for 10 min. Cellular viability was tested using the trypan blue exclusion method, and it was considered satisfactory when the viability was over 95%.

Bone marrow-derived hematopoietic stem cells isolation

PBS supplemented with 10% fetal bovine serum (FBS) was injected into the femurs that were sectioned between the femoral-iliac joint and femur–tibia, to release the stem cell string. Cells were placed in a Falcon tube containing 5 ml of 10% FBS–PBS and carefully mixed to form a homogenous cell suspension. The cell suspensions were transferred to 15-ml Falcon tubes containing 3 ml of Histopaque 1077 (Sigma). Stem cells were then purified as described above. The final cell fraction was resuspended in PBS and cellular viability was tested using the trypan blue exclusion method, and it was considered satisfactory when the viability was over 95%.

Fluorimetric ROS measurement

General ROS production was measured by incubating mitochondria (0.5 mg/ml) in standard reaction medium containing 5 μM of 2',7'-dichlorodihydrofluorescein diacetate (H_2DCF-DA) (Molecular Probes, Invitrogen, Carlsbad, CA) at 28°C. DCF fluorescence was monitored using a F4500 spectrofluorometer (Hitachi F4500, Tokyo, Japan) operating at excitation and emission wavelengths of 488 and 525 nm, respectively, slit widths of 2.5 nm, with continuous stirring. In isolated cells (10^5 cells/ml circulating mononuclear and 10^6 cells/ml spleen mononuclear or bone marrow stem cells) and islet (25 islet/ml), the production of ROS was determined by incubating them with Hanks balanced salt solution medium containing 5 μM of H_2DCF-DA at 37°C.

Hydrogen peroxide production was measured by incubating mitochondria (0.5 mg/ml) in standard reaction medium containing 10 μM of Amplex Red (Molecular Probes, Invitrogen, Carlsbad, CA) and 1 U/ml of horseradish peroxidase at 28°C. Resorufin fluorescence was monitored using a RF5301 spectrofluorometer (Shimatsu PC, Kyoto, Japan) operating at excitation and emission wavelengths of 563 and 587 nm, respectively, slit widths of 5 nm, with continuous stirring.

Flow cytometry ROS measurement

Mitochondrial superoxide generation was assessed using MitoSOX™ Red, a highly selective fluorescent probe for the detection of superoxide generated within mitochondria. MitoSOX™ Red was added to the cells (10^5 cells ml^{-1} circulating mononuclear and 10^6 cells ml^{-1} spleen mononuclear or bone marrow stem cells) at a final concentration of 5 μM in culture media and incubated at 37°C for 10 min. The cells were then washed with RPMI 1640 medium (Invitrocell). Fluorescence intensity was analyzed using a FACSCalibur flow cytometer (BD Biosciences, San Jose, CA, USA) equipped with an argon laser and CellQuest software (version 4.1) with excitation at 488 nm and emission at 620 nm. A minimum of 10,000 events were collected. Results are presented as single-parameter histograms or scattergrams of cellular events versus fluorescence intensity [31].

Skeletal muscle and liver oxygen consumption

Fragments (3–5 mg) of soleus muscle and liver were placed in a Petri dish on ice with 1 ml of relaxing solution [containing 10mM of Ca-EGTA buffer (2.77 mM of CaK2EGTA + 7.23 mM of K2EGTA), 0.1 mmol/L of free concentration of calcium, 20 mmol/L of imidazole, 50 mmol/L of K+/4-morpholinoethanesulfonic acid, 0.5 mmol/L of dithiothreitol, 7 mmol/L of MgCl2, 5 mmol/L of ATP, 15 mmol/L of phosphocreatine, pH = 7.1]. Soleus skeletal muscle fiber bundles were separated using two forceps. Tissue samples were permeabilized for 30 min in ice-cold relaxing solution with saponin (50 μg/mL), gently stirred, and washed 3 times with MiR05 medium [60 mmol/L of potassium lactobionate, 0.5 mmol/L of EGTA, 3 mmol/L of MgCl2, 20 mmol/L of taurine, 10 mmol/L of KH2PO4, 20 mmol/L of Hepes, 110 mmol/L of sucrose, 1 g/L of BSA, pH = 7.1] at 4°C. Tissue samples were then immediately transferred into an Oroboros respirometer (Innsbruck, Austria) containing an air-saturated respiration medium, MiR05, in the presence of pyruvate (10 mM) and malate (5 mM). The respiration rate in state III was measured after addition of ADP (400 μM), the state IV in the presence of oligomycin (1.0 μg/ml) and at last the uncoupler Carbonyl cyanide-4-(trifluoromethoxy)phenylhydrazone (FCCP) was added (0.2 μM to liver and 1.5 μM to muscle). The Oxygraph-2k (Oroborus, Innsbruk, Austria) is a two-chamber titration-injection respirometer with a limit of oxygen flux detection of 1.0 pmol/sec/ml, at 37°C.

CS activity

Citrate synthase (CS) activity was assayed by measuring the conversion of oxaloacetate and acetyl-CoA to citrate and SH-CoA catalyzed by CS and monitoring the colorimetric product, thionitrobenzoic acid, as described by Shepherd and Garland [32]. Briefly, liver, muscle, or islet tissues were homogenized (1:10, W:V) in 50 mM of Tris-buffer, 1 mM of EDTA, and 5% Triton X-100, at pH = 7.4. After centrifugation at 700 g for 10 min, supernatant was saved and further diluted in 50 mM of Tris-buffer to a final concentration of ~1 mg/ml. Four to six micrograms of proteins of these samples was added to a microplate before adding 250 uL of CS reaction buffer (50 mM of Tris-HCl (pH = 8.0), 0.1% Triton X-100, 250 μM of oxaloacetate, 50 μM of acetyl-CoA, and 100 μM of 5,5′-dithiobis(2-nitrobenzoic acid)). The kinetics of absorbance at 412 nm was measured in a microplate reader (PowerWave XS 2,

BioTek) for 6 min. The enzyme activity was calculated as µmol of citrate formation per min, and expressed per mg of sample protein (U/mg).

Sample preparation and MALDI-MS analysis

Mitochondrial extracts were diluted in a 10 mg/mL solution of α-cyano-hydroxycinnamic acid in MeOH:ACN (acetonitrile) (50:50) to a proportion of 1:100. A volume of 1.5 µL of this mixture was transferred to a MALDI 96-well plate and then sent to analysis after homogenous crystallization. Mass spectrometric data were acquired in a MALDI-LTQ-XL quadrupole linear trap instrument (Thermo Scientific, San Jose, CA, USA) equipped with a solid-state Nd:YAG laser. Typical operating conditions were as follows: 4.0 µJ of laser energy, 3 shots per step, *m/z* range of 50–1000, and negative ion mode. For structural elucidation, collision-induced dissociation (CID) reactions (MS/MS) were performed using helium as the buffer gas with 30–50 normalized energy. The obtained data from all replicates and groups were submitted to a principal component analysis (PCA) using the Unscrambler software (v. 9.7, CAMO software, Oslo, Norway) for identifying chemical markers that could indicate each condition. Once elected, the markers were submitted to MS/MS reactions and the obtained fragments were compared with those generated by simulations on Mass Frontier software (v. 6.0, Thermo Scientific, San Jose, CA, USA). When all the observed fragments matched the simulated ones, the structure can be assigned to that particular *m/z*.

Statistical analyses

Two mean comparisons within each age group were tested by Student's t-test, using GraphPad Prism 5 software. Data are presented as Average ± SE of independent experiments. Differences were considered significant when p value was less than 0.05.

Results

In this work, NOD mice mitochondrial (dys)functions were studied in several tissues (liver, muscle, mononuclear and stem cells, and pancreatic islets) in three stages of diabetes development, namely, 4–6 weeks of age (non-diabetic, glycemia: <100 mg/dl), 7–10 weeks of age (pre-diabetic, glycemia: 100–150 mg/dl), and 14–25 weeks of age (diabetic glycemia >250 mg/dl) as compared with age-matched control Balb/c mice.

Mitochondrial respiratory activities are presented in liver (Figure 1, panel A) and skeletal muscle (Figure 1, panel B) under resting (oligomycin A), phosphorylating (ADP), and uncoupled (FCCP) states in permeabilized tissue biopsies. The results were normalized by the CS activity (pmol O_2/s/mU) and demonstrate that, regardless of the stage of the disease, there were no significant differences between NOD and Balb/c mice respiratory activities in both tissues. These results are in agreement with those obtained in isolated mitochondria from the liver of non-diabetic, pre-diabetic, and diabetic NOD and age-matched Balb/c mice (Table I). It was observed that in muscle biopsies, CS activity decreased by 32% after the onset of the disease (Table II). This suggests that T1D reduces the amount of functional mitochondria in muscle, but not in liver.

Since apoptosis can be triggered by MPT, we assessed the susceptibility of NOD mice mitochondria to this process by analyzing Ca^{2+}-induced mitochondrial swelling and the ability of mitochondria to retain the accumulated

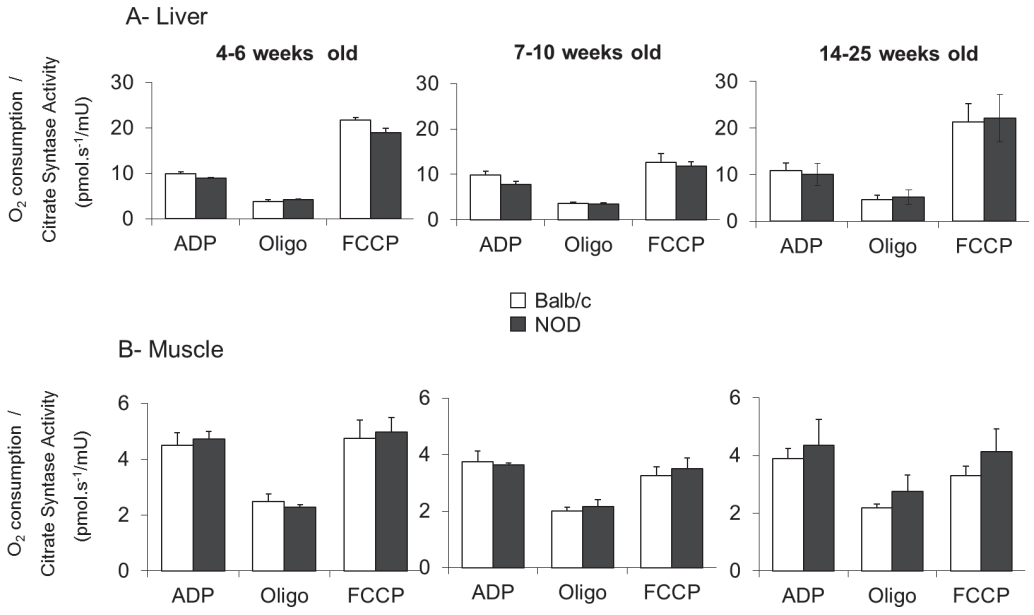

Figure 1. Mitochondrial respiration rates (oxygen consumption) in liver (A) and skeletal muscle (B) biopsies are not altered in NOD mice before and during development of diabetes. Tissue biopsies (2–3 mg) were added to the MiR05 medium. The following were added: 400 µM of ADP, 1 mg/ml of oligomycin, and 0.2 µM of FCCP for liver or 1.5 µM of FCCP for skeletal muscle. Data are mean ± SE of five independent experiments.

Table I. Oxygen consumption rates in isolated mitochondria from liver of NOD and age-matched Balb/c mice measured in phosphorylating state (State III) and resting state (State IV).

	4–6 weeks old (non-diabetic)		7–10 weeks old (pre-diabetic)		14–25 weeks old (diabetic)	
Oxygen consumption (nmol O_2/min/mg)	Balb/c $n=8$	NOD $n=8$	Balb/c $n=11$	NOD $n=12$	Balb/c $n=16$	NOD $n=16$
State III	51.6 ± 1.1	54.6 ± 1.8	45.4 ± 2.6	51.4 ± 2.0	46.2 ± 1.3	44.2 ± 1.2
State IV	9.6 ± 0.3	11.0 ± 0.3	9.0 ± 0.5	10.2 ± 0.4	9.4 ± 0.2	8.8 ± 0.3
RC (state III/state IV)	5.4 ± 0.3	5.0 ± 0.3	5.0 ± 0.3	5.1 ± 0.3	4.9 ± 0.2	5.2 ± 0.3

Average ± SE. RC− respiratory control. State III: upon addition of 200 nM of ADP.

cation. Figure 2 shows that in all stages of the disease, NOD liver mitochondria exhibit extensive cyclosporin-A-sensitive swelling, in contrast to the liver mitochondria isolated from Balb/c mice. Accordingly, the changes in Ca^{2+} Green fluorescence shown in Figure 3 indicate that NOD liver mitochondria retain Ca^{2+} for a much shorter period of time than Balb/c mitochondria, irrespective of the disease stages. Balb/c mitochondria are able to retain calcium 3–5 folds longer than NOD mitochondria. These results indicate that NOD liver mitochondria present increased susceptibility to Ca^{2+}-induced MPT that is not related to the increasing levels of glycemia.

It is well known [33,34] that ROS play an important role in the MPT pore opening. Therefore, we estimated ROS production using two different probes: Amplex Red, a specific probe for hydrogen peroxide and H_2DCF-DA that detects a large variety of reactive oxygen and nitrogen species [35], and is also used to indicate cell death associated with oxidative stress [36]. The analyses of fluorescence changes in both probes, H_2DCF-DA (Figure 4A) and Amplex Red (Figure 4B), induced by liver mitochondria isolated from NOD or Balb/c indicate that only the NOD mitochondria isolated from non-diabetic NOD mice present higher rates of ROS release. The data suggest that H_2O_2 production or elimination rates are significantly altered in mitochondria from NOD at the initial, non-diabetic stage. Interestingly, in more advanced stages of diabetes, differences in H_2O_2 production rates between NOD and Balb/c liver mitochondria are not detected.

Since T1D is an autoimmune disease involving lymphocyte activation [22,23,37], we also investigated ROS production in spleen and circulating mononuclear cells and their precursor stem cells. Hematopoietic stem cells can be differentiated into lymphoid cells such as T and B lymphocytes that are involved in the development of T1D [38,39]. In these experiments we used, in addition to H_2DCF-DA, the MitoSOX, a marker for mitochondrial superoxide production in intact cells [40,41]. Higher levels of H_2DCF-DA oxidation occurred in all cell types at all diabetic stages of NOD mice as compared with those in age-matched Balb/c cells. These results were not proportional to increasing glycemia levels in the mice (Figure 5A–C). In contrast to H_2DCF-DA data, MitoSOX fluorescence did not differ between NOD and Balb/c spleen mononuclear (Figure 6A), circulating mononuclear (Figure 6B), as well as hematopoietic stem cells (Figure 6C), at all stages of the disease. These results suggest that immune cell oxidative stress detected by the oxidation of H_2DCF-DA probably does not come from mitochondrial source measured by MitoSOX.

Macrophage infiltration into the pancreatic islets from NOD is an early event related to islet destruction [22,23]. Therefore, we evaluated H_2DCF-DA oxidation using isolated pancreatic islets from non-diabetic NOD mice (Figure 7A). Mice with 4 weeks of age were used to obtain islets with low-grade cellular infiltration. H_2DCF-DA oxidation was sevenfold higher in islets from NOD than that in islets from Balb/c mice (Figure 7B). To evaluate if the exacerbated probe oxidation in NOD islets was related to the content of mitochondria, we measured the total CS activity. No differences were observed in CS activity in islets from non-diabetic NOD and Balb/c mice (Figure 7C), indicating similar number of functional mitochondria in islets from both groups at this early age.

In order to reinforce the ROS probes data, we investigated the presence of oxidative damaged macromolecules (lipids) in isolated liver mitochondria of NOD mice (Table III). Using MALDI mass spectrometry and the lipidomics approach, we identified oxidized lipid markers, most of them being derivatives of diacylglycerols and phospholipids, in NOD liver mitochondria for each disease stage.

Table II. CS activity in biopsies of liver and soleus muscle from NOD and age-matched Balb/c mice.

	4–6 weeks old (non-diabetic)		7–10 weeks old (pre-diabetic)		14–25weeks old (diabetic)	
Citrate synthase activity (mU/mg of tissue)	Balb/c	NOD	Balb/c	NOD	Balb/c	NOD
Liver	3.4 ± 0.7	3.6 ± 0.2	2.8 ± 0.2	2.9 ± 0.6	2.5 ± 0.6	2.3 ± 0.7
Muscle	8.8 ± 1.7	9.0 ± 1.7	9.3 ± 0.3	9.3 ± 1.1	9.4 ± 1.3	6.4 ± 1.9 *

Average ± SE. Student's t-test: $^*p<0.05$.

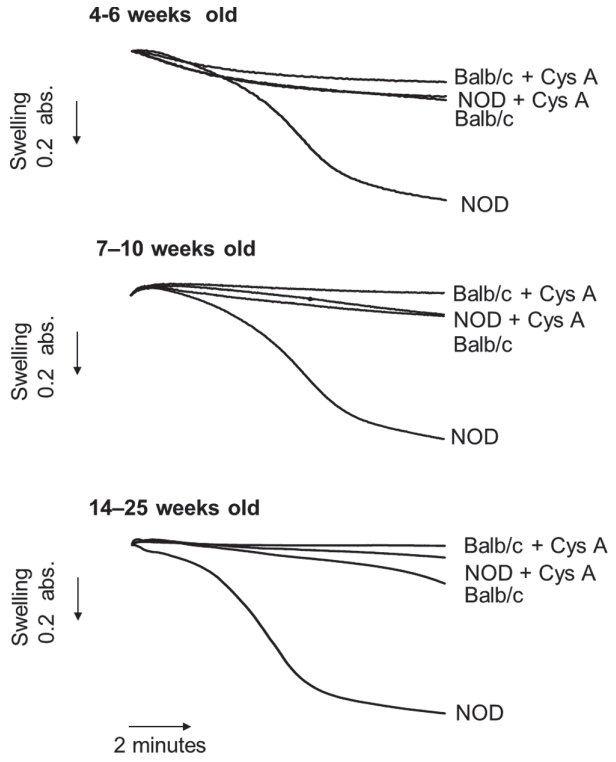

Figure 2. Liver mitochondrial susceptibility to calcium-induced swelling is markedly increased in NOD mice before and during development of diabetes. Mitochondria (0.5 mg/ml) were incubated in standard medium at 28°C with addition of 60 μM of Ca^{2+}. Absorbances at 10 minutes for Balb/c vs. NOD were non-diabetic group: 1.1 ± 0.2 versus 0.86 ± 0.1; pre-diabetic group: 1.06 ± 0.2 versus 0.82 ± 0.1; diabetic group: 1.3 ± 0.3 versus 1.02 ± 0.3. $p < 0.05$ for all comparisons. Data are Average ± SE of eight independent experiments.

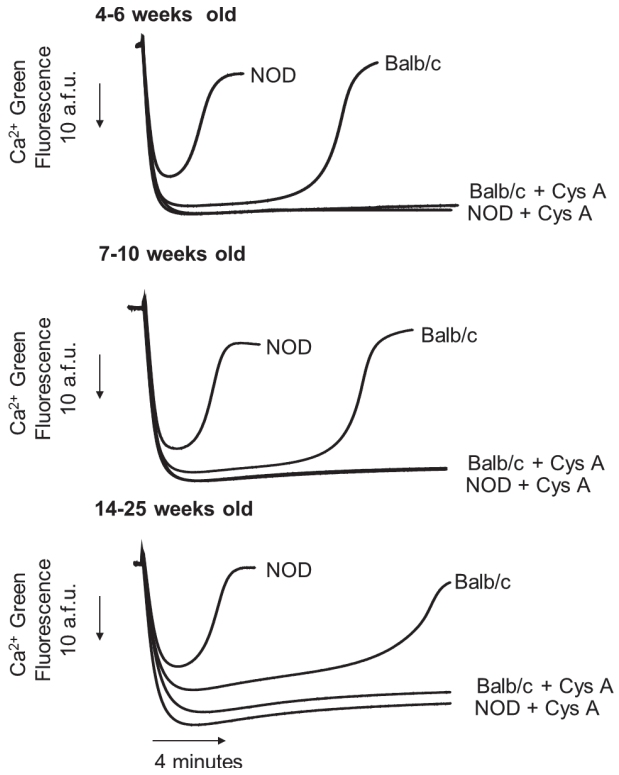

Figure 3. Liver mitochondrial calcium retention capacity is profoundly reduced in NOD mice before and during the development of diabetes. Mitochondria (0.5 mg/ml) were incubated in standard medium at 28°C with 0.1 μM of calcium green in 5 N of hexapotassium salt. Figure representative of five independent experiments performed in duplicate. Average times (seconds) for calcium release for Balb/c versus NOD were non-diabetic group: 972.2 ± 122.0 versus 349.2 ± 132.9; pre-diabetic group: 670.8 ± 151.8 versus 244.5 ± 96.6; diabetic group: 968.9 ± 28.5 versus 182.8 ± 11.9; $P < 0.05$ for all comparisons.

Discussion

In the present study, we analyzed mitochondrial function in metabolic organs such as liver, skeletal muscle, and pancreatic islets and also in the main cells involved in autoimmune diseases (mononuclear cells) along the three phases of T1D development: before, during, and after β-cell destruction in NOD compared with control Balb/c mice.

In *in vitro* standard optimum conditions, oxygen consumption by isolated mitochondria and tissue biopsies were not altered during T1D development in NOD compared with matched control mice. In addition, the number of functional mitochondria in liver biopsies was not altered. Herlein et al. [42] also showed no alterations in mitochondrial respiration in liver mitochondria of streptozotocin-diabetic rats. However, in muscle biopsies from diabetic NOD mice, there was a significant decrease in the indicator of functional mitochondria number, CS activity. This finding is supported by previous study [43] that showed altered mitochondrial biogenesis, structure, and function in muscle tissue from diet-induced diabetic mice.

The susceptibility of mitochondria to undergo permeability transition (MPT) in physiological and stressful conditions is directly associated with redox imbalance and the intrinsic pathway of cell death [5]. After about 40 years of research, the importance of MPT in mammalian cell fate has been well recognized, especially after numerous observations that MPT blockers prevent cell death in many disease models [34]. Here, we observed that liver mitochondria susceptibility to calcium-induced MPT was markedly increased in organelles obtained from NOD mice, before and during the development of T1D compared with controls of the same age. This MPT predisposition was assessed by measuring the organelle swelling (increased in NOD, Figure 2) and the calcium retention capacity (reduced in NOD, Figure 3). The calcium signaling to MPT is highly relevant in cell death processes. Mitochondria *in situ* may be exposed to high concentrations of calcium released directly from the endoplasmic reticulum (ER), the main intracellular calcium storage (250–600 uM), and independent of variations in cytoplasm calcium concentrations [44,45]. This process is mediated by a physical interaction between ER and mitochondria through a membrane structure known as "mitochondria-associated membranes", which is composed of proteins that bridge the two organelles enabling the direct transfer of Ca^{2+} from ER to mitochondria. For example, the

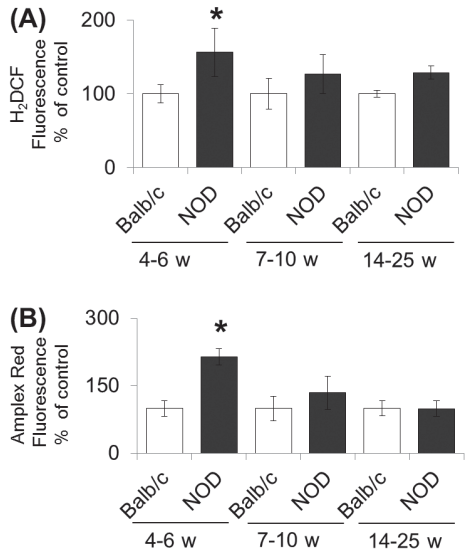

Figure 4. Liver mitochondrial global ROS (H_2DCF-DA oxidation) and H_2O_2 generation (Amplex Red) are increased in non-diabetic NOD mice, but not in later stages of diabetes development. Mitochondria from NOD and Balb/c mice (0.5 mg/ml) were incubated in standard medium at 28°C, in the presence of 1μM of H_2DCF-DA (A), 10 μM of Amplex Red, 1 U/ml of horseradish peroxidase (B), and 10 μM of Ca^{2+}. The results are expressed in percentage relative to the control. Data are the Average ± SE of eight independent experiments. *$p \leq 0.05$ NOD *versus* Balb/c (Student's t-test).

protein grp75 connects the Inositol trisphosphate (IP3) ER receptor with the voltage-dependent anionic channel in mitochondria [46]. Mitochondrial dysfunction such as the opening of permeability transition pore may be a general event with widespread tissue occurrence in T1D, since there is a close interrelationship between oxidative stress and inflammatory signaling pathways [47].

We conducted several experiments in isolated mitochondria and in intact cells to estimate the ROS production which is closely linked with calcium-induced MPT [34]. Our results indicate that mitochondrial ROS (DCF) and H_2O_2 (Amplex Red) release increased in liver mitochondria of non-diabetic NOD mice, but not in advanced stages of the disease (Figure 4). Herlein et al. [42] also observed no changes in H_2O_2 production in liver mitochondria from streptozotocin-diabetic rats. The increased H_2O_2 production by liver mitochondria of non-diabetic NOD mice observed in the present study could be explained by the activation of macrophages and lymphocytes at this early stage of the disease [1,4,23], which leads to a generalized inflammation, including liver tissue, rich in Kupffer cells. The fact that increased H_2O_2 release in isolated mitochondria is detected only in the early but not in more advanced stages of the disease may be related to a homeostatic response of upregulation of mitochondrial antioxidant system in face of a chronic oxidative insult. Nonetheless, when the cell (but not mitochondria) oxidative stress persists, the organelles are attacked by the extra-mitochondrial generated ROS. If this assumption is true, we should be able to detect mitochondrial oxidative damage, such as lipoperoxides, in the later stages. In fact, lipidomic analyses evidenced the presence of oxidized lipid in liver mitochondria of all 3 stages of the disease. Oxidized polyunsaturated fatty acids in mitochondrial cardiolipin and other phospholipids disturb membrane integrity and are associated with the early phase of apoptosis [48]. Alterations of mitochondrial cardiolipin are thought to be involved in the development of diabetes and other pathologic conditions [49,50].

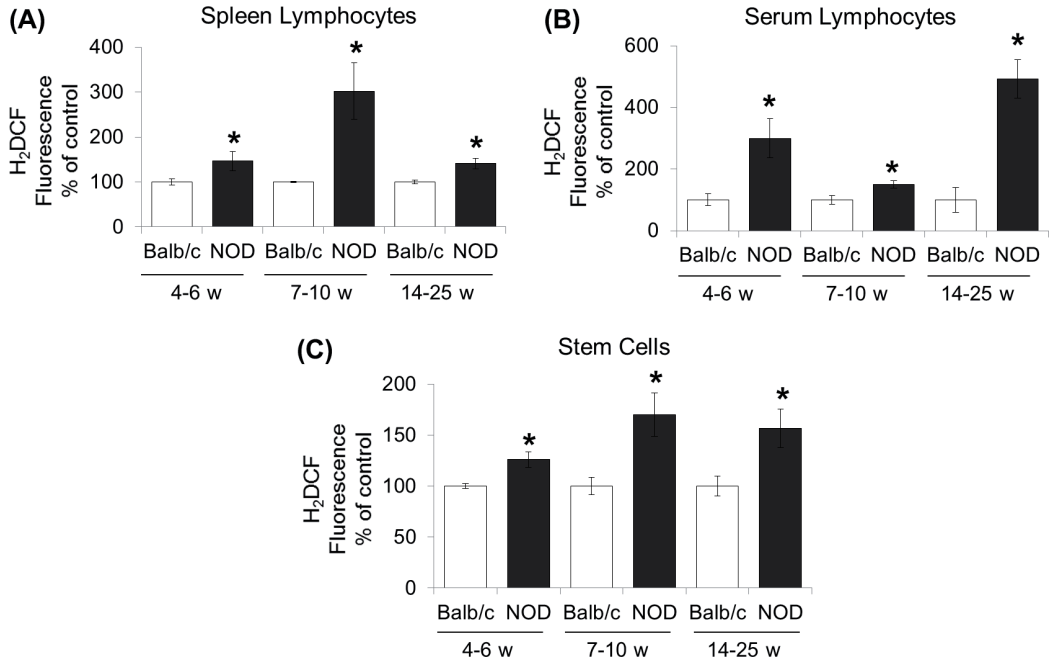

Figure 5. ROS production (H_2DCF-DA oxidation) is increased in intact mononuclear and stem cells from NOD mice before and during diabetes development. 1×10^6 cells for spleen mononuclear (A), 1×10^5 cells for circulating mononuclear (B), and 1×10^6 stem cells (C) were incubated in Hank's balanced salt solution (HBSS) medium in the presence of 1μM of H_2DCF-DA. The results are expressed in percentage relative to the control. Data are the Average ± SE of five independent experiments. *$p \leq 0.05$ NOD *versus* Balb/c (Student's t-test).

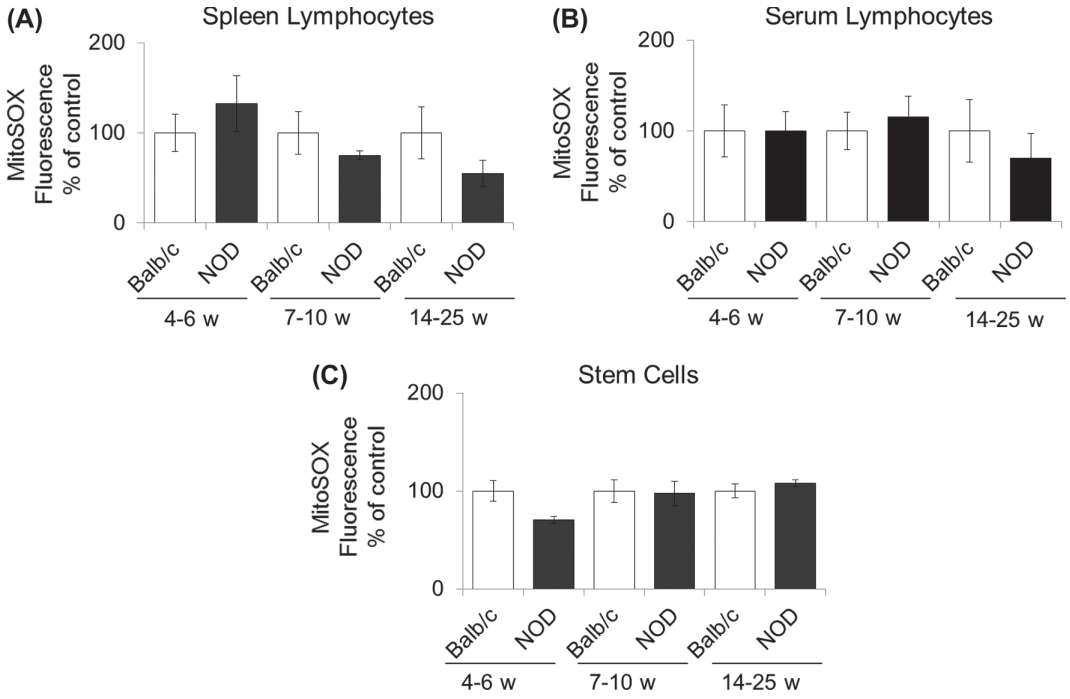

Figure 6. Mitochondrial superoxide production (MitoSox) is not altered in intact mononuclear and stem cells from NOD mice along the development of diabetes. 1×10^6 cells for spleen mononuclear (A), 1×10^5 cells for circulating mononuclear (B), and 1×10^6 stem cells (C) were incubated in RPMI 1640 medium in the presence of 5 μM of MitoSOX Red. The results are expressed in percentage relative to the control. Data are the Average ± SE of five independent experiments. *$p \leq 0.05$ NOD *versus* Balb/c (Student's t-test).

Bao et al. [51] demonstrated that insulin-secreting cells accumulated oxidized phospholipid molecular species and exhibited higher levels of apoptosis when treated with streptozotocin or inflammatory cytokines.

Intact mononuclear cells from peripheral blood and from spleen and stem cells from bone marrow of NOD mice exhibited increased oxidation of the probe H_2DCF-DA before and during diabetes development (Figure 5). This could not only be the result of a direct action of ROS and RNS on the probe, but also may reflect the cell damage caused by the oxidative stress, for example, the leak of iron and cytochrome c from damaged mitochondria to

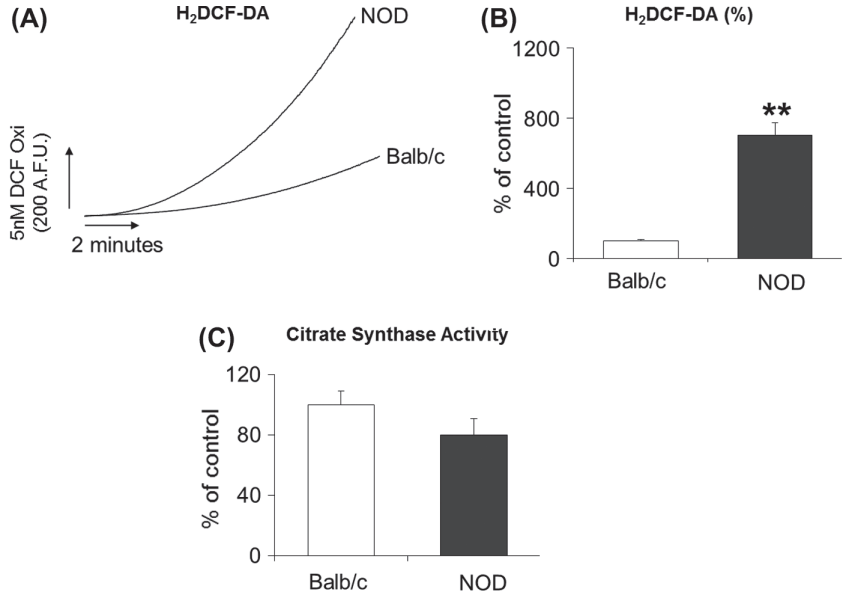

Figure 7. ROS production (H_2DCF-DA oxidation) and CS activity in isolated pancreatic islets from non-diabetic NOD mice (4 weeks of age) compared with islets from age-matched Balb/c mice. Islets were incubated in HBSS medium in the presence of 1μM of H_2DCF-DA. Representative trace of three independent experiments (A), and results expressed in percentage relative to the control (B). Data are Average ± SE of three independent experiments with 25 islets in each. CS activity from isolated pancreatic islets (C). Data are Average ± SE of eight independent experiments with 25 islets each. *$p \leq 0.05$ NOD *versus* Balb/c (Student's t-test).

Table III. Oxidized lipid markers identified in liver mitochondria from NOD and age-matched control (Balb/c) mice by MALDI-MS and PCA.

Group	Molecule class	CN:DB[a]	[M - H]$^-$ *m/z*	CID products *m/z*
Control (Balb/c, all ages)	Diacylglycerol	28:0	511	493, 467, 423
	Diacylphosphoglycerol	35:5	679	661, 635, 489
	Phosphatidylcholine	36:4	738	720, 694, 677
Non-Diabetic	Oxidized diacylglycerol	34:3	605	561, 517, 473
	Oxidized diacylglycerol	33:4	589	545, 501, 400
	Oxidized glycerophosphatidylglycerol	20:5	545	527, 501, 457
Pre-Diabetic	Oxidized phosphatidylcholine	46:1	991	975, 949, 865
	Oxidized diacylglycerol	34:3	621	603, 577, 432
	Diacylglycerol	30:2	567	549, 523
Diabetic	Oxidized phosphatidylcholine	34:4	785	767, 741, 438
	Oxidized phosphatidylserine	42:4	883	864, 703
	Lyso-α-D-glucopyranosylcardiolipin	52:0	1327*	1309, 1081, 847

[a]Carbon number: Double bond.
*As described in Ref [61].

cytosol leading to cell death [36]. Therefore, DCF fluorescence evidences the oxidative stress or damage in immune cells from NOD mice in early and advanced diabetic stages. Accordingly, Kim et al. [52] showed evidence of increased H_2O_2 generation (dihydrorhodamine oxidation) by T lymphocytes and monocytes in the peripheral blood of obese Zucker rats before the development of diabetes.

The specific mitochondrial generation of superoxide (MitoSOX) was not altered in mononuclear and stem cells isolated from NOD mice before and during diabetes development (Figure 6). Herlein et al. [42] also showed no changes in superoxide production by mitochondria isolated from muscle, heart, and liver of streptozotocin-diabetic rats. The authors proposed that these results may reflect an adaptive response of mitochondria to the oxidative stress, for instance, through increases in antioxidant enzymes or uncoupling protein 3 (UCP-3) activity. In addition, another study [52] reported no changes in superoxide production in spleen lymphocytes from obese not-as-yet diabetic Zucker rats. Therefore, we suggest that mitochondria are not an important source of ROS in immune cells of NOD mice. Instead, mitochondria may be a target of ROS generated in extra-mitochondrial compartments.

The pancreatic islets isolated from non-diabetic NOD mice (4 weeks old) showed markedly increased oxidation of H_2DCF, while the amount of functional mitochondria (CS activity) was not altered (Figure 7). At this stage that precedes the onset of disease, there is hypersecretion of insulin due to the increased volume of β-cells in response to increased pro-inflammatory cytokines in pancreatic islets [25]. This is in accordance with the presence of functional mitochondria.

Various inflammatory cytokines and oxidative stress produced by islet-infiltrating immune cells have been proposed to play an important role in mediating the destruction of β-cells. The oxidative stress mechanism and inflammatory signals are interrelated. Pro-inflammatory cytokines signal directly and indirectly to ROS production, for instance, through activation of reduced nicotinamide adenine dinucleotide phosphate (NADPH) oxidase, ER stress, and increases in cellular iron uptake. On the other hand, oxidative stress provokes inflammatory responses through activation of c-Jun N-terminal kinase (JNK), nuclear factor kappa B (NF-kB), and p38 mitogen-activated protein kinase pathway. Therefore, a positive feedback loop is likely to occur in the β-cell (and perhaps in other tissues) in which inflammatory mediators promote ROS generation that activates transcription of various cytokines, which in turn act in an autocrine manner to exacerbate the oxidative and inflammatory responses. Intracellularly, there is an extensive crosstalk between signaling molecules involved in oxidative stress, ER stress, inflammatory responses, and mitochondrial dysfunction. This issue has been excellently reviewed by Imai et al. [47].

The present study has shown that the mononuclear and stem cells from NOD mice present increased ROS production and ROS-induced damage and that NOD mitochondria are more susceptible to permeability transition pore opening as compared with Balb/c mice, before and during diabetes development. These events may occur due to different factors at each stage of the disease progress. In the initial stage (non-diabetic) of auto-immune diseases, infiltration of activated T lymphocytes into target tissues induces activation of resident macrophages and recruitment of circulating monocytes. The activated macrophages produce pro-inflammatory cytokines and ROS, mainly through activation of NADPH oxidase [53,54]. Intracellular ROS signals calcium release [55,56], which then would contribute to mitochondria dysfunction (increased susceptibility to permeability transition).

In the pre-diabetic stage, an increase in intracellular Ca^{2+} concentration is observed in β-cells of NOD mice [25], probably due to a lower expression of sarco/ER calcium ATPase compared with those of control mice. The increased intracellular Ca^{2+} maintains increased insulin secretion, a feature of this stage of pre-diabetes. The elevated intracellular Ca^{2+} levels will trigger both mitochondria MPT and generation of ROS.

In the diabetic stage, hyperglycemia leads to the formation of advanced glycation end products (AGEs). These AGEs are able to induce several abnormal responses in vivo, such as increased expression of NF-κB, secretion of pro-inflammatory cytokines, alterations of mitochondrial respiratory chain proteins, and mitochondrial DNA damage and apoptosis of different cell types [57–59]. AGEs may also increase the expression and activity of NADPH oxidase and deplete the antioxidant system contributing to the formation of free radicals [59]. Increases in AGEs [60] and TNF-α and IL-1 [59] are found in the serum of patients with T1D [60]. It was previously demonstrated that the AGEs in the diet can anticipate the onset of diabetes in NOD, db/db, and apolipoprotein E knockout mice [57].

The present study shows that, in the T1D NOD mouse model, the oxidative insult that triggers mitochondrial permeability transition is generated in the extra-mitochondrial compartment, occurs in several tissues, and starts much before the onset of the disease.

Declaration of interest

The authors report no conflicts of interest. The authors alone are responsible for the content and writing of the paper.

This study was supported by grants obtained by HCFO and AEV from the Brazilian agencies: Fundação de Amparo a Pesquisa do Estado de São Paulo (FAPESP # 2011/50400–0 and 2011/51349-8) and Conselho Nacional de Desenvolvimento Científico e Tecnológico (CNPq). CM, PGG, ACRL, and DNO were supported by Coordenação de Aperfeiçoamento de Pessoal de Nível Superior (CAPES) fellowships.

Acknowledgements

We thank Ms. Natalia Mayumi Inada, Edilene de Souza Siqueira Santos, and Conceição Aparecida Vilella for the technical assistance.

References

[1] Delmastro MM, Piganelli JD. Oxidative stress and redox modulation potential in type 1 diabetes. Clin Dev Immunol 2011;2011:593863.

[2] Rabinovitch A, Suarez-Pinzon WL, Strynadka K, Lakey JR, Rajotte RV. Human pancreatic islet beta-cell destruction by cytokines involves oxygen free radicals and aldehyde production. J Clin Endocrinol Metab 1996;81:3197–3202.

[3] Augstein P, Elefanty AG, Allison J, Harrison LC. Apoptosis and beta-cell destruction in pancreatic islets of NOD mice with spontaneous and cyclophosphamide-accelerated diabetes. Diabetologia 1998;41:1381–1388.

[4] Barthson J, Germano CM, Moore F, Maida A, Drucker DJ, Marchetti P, et al. Cytokines tumor necrosis factor-alpha and interferon-gamma induce pancreatic beta-cell apoptosis through STAT1-mediated Bim protein activation. J Biol Chem 2011;286:39632–39643.

[5] Gurzov EN, Eizirik DL. Bcl-2 proteins in diabetes: mitochondrial pathways of beta-cell death and dysfunction. Trends Cell Biol 2011;21:424–431.

[6] Thomas HE, McKenzie MD, Angstetra E, Campbell PD, Kay TW. Apoptosis. Beta cell apoptosis in diabetes. Apoptosis 2009;14:1389–1404.

[7] Kowaltowski AJ, de Souza-Pinto NC, Castilho RF, Vercesi AE. Mitochondria and reactive oxygen species. Free Radic Biol Med 2009;47:333–343.

[8] Vercesi AE, Castilho RF, Kowaltowski AJ, Oliveira HC. Mitochondrial energy metabolism and redox state in dyslipidemias. IUBMB Life 2007;59:263–268.

[9] Kowaltowski AJ, Vercesi AE. Mitochondrial damage induced by conditions of oxidative stress. Free Radic Biol Med 1999;26:463–471.

[10] Kowaltowski AJ, Castilho RF, Vercesi AE. Mitochondrial permeability transition and oxidative stress. FEBS Lett 2001; 495:12–15.

[11] Skulachev VP. Cytochrome c in the apoptotic and antioxidant cascades. FEBS Lett 1998;423:275–280.

[12] Leite AC, Oliveira HC, Utino FL, Garcia R, Alberici LC, Fernandes MP, et al. Mitochondria generated nitric oxide protects against permeability transition via formation of membrane protein S-nitrosothiols. Biochim Biophys Acta 2010;1797:1210–1216.

[13] Brookes PS, Salinas EP, Darley-Usmar K, Eiserich JP, Freeman BA, Darley-Usmar VM, Anderson PG. Concentration-dependent effects of nitric oxide on mitochondrial permeability transition and cytochrome c release. J Biol Chem 2000;275:20474–20479.

[14] Lemasters JJ, Theruvath TP, Zhong Z, Nieminen AL. Mitochondrial calcium and the permeability transition in cell death. Biochim Biophys Acta 2009;1787:1395–1401.

[15] Oliveira HC, Cosso RG, Alberici LC, Maciel EN, Salerno AG, Dorighello GG, et al. Oxidative stress in atherosclerosis-prone mouse is due to low antioxidant capacity of mitochondria. FASEB J 2005;19:278–280.

[16] Alberici LC, Oliveira HC, Bighetti EJ, de Faria EC, Degaspari GR, Souza CT, Vercesi AE. Hypertriglyceridemia increases mitochondrial resting respiration and susceptibility to permeability transition. J Bioenerg Biomembr 2003;35: 451–457.

[17] Alberici LC, Oliveira HC, Paim BA, Mantello CC, Augusto AC, Zecchin KG, et al. Mitochondrial ATP-sensitive K(+) channels as redox signals to liver mitochondria in response to hypertriglyceridemia. Free Radic Biol Med 2009;47:1432–1439.

[18] Paim BA, Velho JA, Castilho RF, Oliveira HC, Vercesi AE. Oxidative stress in hypercholesterolemic LDL (low-density lipoprotein) receptor knockout mice is associated with low content of mitochondrial NADP-linked substrates and is partially reversed by citrate replacement. Free Radic Biol Med 2008;44:444–451.

[19] Figueira TR, Castilho RF, Saito A, Oliveira HC, Vercesi AE. The higher susceptibility of congenital analbuminemic rats to Ca2+-induced mitochondrial permeability transition is associated with the increased expression of cyclophilin D and nitrosothiol depletion. Mol Genet Metab 2011;104:521–528.

[20] Martinez-Abundis E, Rajapurohitam V, Haist JV, Gan XT, Karmazyn M. The obesity-related peptide leptin sensitizes cardiac mitochondria to calcium-induced permeability transition pore opening and apoptosis. PLoS One 2012;7:e41612.

[21] Huhn R, Heinen A, Hollmann MW, Schlack W, Preckel B, Weber NC. Cyclosporine A administered during reperfusion fails to restore cardioprotection in prediabetic Zucker obese rats in vivo. Nutr Metab Cardiovasc Dis 2009;20:706–712.

[22] Makino S, Kunimoto K, Muraoka Y, Mizushima Y, Katagiri K, Tochino Y. Breeding of a non-obese, diabetic strain of mice. Jikken Dobutsu 1980;29:1–13.

[23] Anderson MS, Bluestone JA. The NOD mouse: a model of immune dysregulation. Annu Rev Immunol 2005;23: 447–485.

[24] Babad J, Geliebter A, DiLorenzo TP. T-cell autoantigens in the non-obese diabetic mouse model of autoimmune diabetes. Immunology 2010;131:459–465.
[25] Liang K, Du W, Zhu W, Liu S, Cui Y, Sun H, et al. Contribution of Different Mechanisms to Pancreatic Beta-cell Hypersecretion in Non-obese Diabetic (NOD) Mice during Pre-diabetes. J Biol Chem 2011;286:39537–39545.
[26] Kikutani H, Makino S. The murine autoimmune diabetes model: NOD and related strains. Adv Immunol 1992;51:285–322.
[27] Ventura-Oliveira D, Vilella CA, Zanin ME, Castro GM, Moreira Filho DC, Zollner RL. Kinetics of TNF-alpha and IFN-gamma mRNA expression in islets and spleen of NOD mice. Braz J Med Biol Res 2002;35:1347–1355.
[28] Kaplan RS, Pedersen PL. Characterization of phosphate efflux pathways in rat liver mitochondria. Biochem J 1983; 212:279–288.
[29] Murphy AN, Bredesen DE, Cortopassi G, Wang E, Fiskum G. Bcl-2 potentiates the maximal calcium uptake capacity of neural cell mitochondria. P Natl Acad Sci USA 1996;93:9893–9898.
[30] Degasperi GR, Velho JA, Zecchin KG, Souza CT, Velloso LA, Borecky J, et al. Role of mitochondria in the immune response to cancer: a central role for Ca $^{2+}$. J bioenerg biomembr 2006;38:1–10.
[31] Payne CM, Weber C, Crowley-Skillicorn C, Dvorak K, Bernstein H, Bernstein C, et al. Deoxycholate induces mitochondrial oxidative stress and activates NF-kappaB through multiple mechanisms in HCT-116 colon epithelial cells. Carcinogenesis 2007;28:215–222.
[32] Shepherd D, Garland PB. The kinetic properties of citrate synthase from rat liver mitochondria. Biochem J 1969;114: 597–610.
[33] Valle VG, Fagian MM, Parentoni LS, Meinicke AR, Vercesi AE. The participation of reactive oxygen species and protein thiols in the mechanism of mitochondrial inner membrane permeabilization by calcium plus prooxidants. Arch Biochem Biophys 1993;307:1–7.
[34] Figueira TR, Barros MH, Camargo AA, Castilho RF, Ferreira JC, Kowaltowski AJ, et al. Mitochondria as a source of reactive oxygen and nitrogen species: from molecular mechanisms to human health. Antioxid Redox Signal 2012; 18:2029–2074.
[35] Kumar S, Patel S, Jyoti A, Keshari RS, Verma A, Barthwal MK, Dikshit M. Nitric oxide-mediated augmentation of neutrophil reactive oxygen and nitrogen species formation: Critical use of probes. Cytometry A 2010;77: 1038–1048.
[36] Karlsson M, Kurz T, Brunk UT, Nilsson SE, Frennesson CI. What does the commonly used DCF test for oxidative stress really show? Biochem J 2010;428:183–190.
[37] Degasperi GR, Denis RG, Morari J, Solon C, Geloneze B, Stabe C, et al. Reactive oxygen species production is increased in the peripheral blood monocytes of obese patients. Metabolism 2009;58:1087–1095.
[38] Herzog EL, Chai L, Krause DS. Plasticity of marrow-derived stem cells. Blood 2003;102:3483–3493.
[39] Fiorina P, Voltarelli J, Zavazava N. Immunological applications of stem cells in type 1 diabetes. Endocr Rev 2011;32: 725–754.
[40] Robinson KM, Janes MS, Beckman JS. The selective detection of mitochondrial superoxide by live cell imaging. Nat Protoc 2008;3:941–947.
[41] Zielonka J, Vasquez-Vivar J, Kalyanaraman B. Detection of 2-hydroxyethidium in cellular systems: a unique marker product of superoxide and hydroethidine. Nat Protoc 2008;3:8–21.
[42] Herlein JA, Fink BD, O'Malley Y, Sivitz WI. Superoxide and respiratory coupling in mitochondria of insulin-deficient diabetic rats. Endocrinology 2009;150:46–55.
[43] Bonnard C, Durand A, Peyrol S, Chanseaume E, Chauvin MA, Morio B, et al. Mitochondrial dysfunction results from oxidative stress in the skeletal muscle of diet-induced insulin-resistant mice. J Clin Invest 2008;118:789–800.
[44] Rizzuto R, Marchi S, Bonora M, Aguiari P, Bononi A, De Stefani D, et al. Ca(2+) transfer from the ER to mitochondria: when, how and why. Biochim Biophys Acta 2009; 1787:1342–1351.
[45] Rizzuto R, De Stefani D, Raffaello A, Mammucari C. Mitochondria as sensors and regulators of calcium signalling. Nat Rev Mol Cell Biol 2012;13:566–578.
[46] Patergnani S, Suski JM, Agnoletto C, Bononi A, Bonora M, De Marchi E, et al. Calcium signaling around Mitochondria Associated Membranes (MAMs). Cell Commun Signal 2011; 9:19.
[47] Imai Y, Dobrian AD, Morris MA, Nadler JL. Islet inflammation:a unifying target for diabetes treatment? Trends Endocrinol Metab 2013;24:351–60.
[48] Ma ZA, Zhao Z, Turk J. Mitochondrial dysfunction and beta-cell failure in type 2 diabetes mellitus. Exp Diabetes Res 2012:703538.
[49] Han X, Yang J, Yang K, Zhao Z, Abendschein DR, Gross RW. Alterations in myocardial cardiolipin content and composition occur at the very earliest stages of diabetes: a shotgun lipidomics study. Biochemistry 2007;46:6417–6428.
[50] Chicco AJ, Sparagna GC. Role of cardiolipin alterations in mitochondrial dysfunction and disease. Am J Physiol Cell Physiol 2007;292:C33–44.
[51] Bao S, Song H, Tan M, Wohltmann M, Ladenson JH, Turk J. Group VIB Phospholipase A(2) promotes proliferation of INS-1 insulinoma cells and attenuates lipid peroxidation and apoptosis induced by inflammatory cytokines and oxidant agents. Oxid Med Cell Longev 2012:989372.
[52] Kim CH, Vaziri ND, Rodriguez-Iturbe B. Integrin expression and H2O2 production in circulating and splenic leukocytes of obese rats. Obesity (Silver Spring) 2007;15: 2209–2216.
[53] Barcellos-de-Souza P, Moraes JA, de-Freitas-Junior JC, Morgado-Diaz JA, Barja-Fidalgo C, Arruda MA. Heme modulates intestinal epithelial cell activation: involvement of NADPHox-derived ROS signaling. Am J Physiol Cell Physiol 2012;304:C170–179.
[54] Gauss KA, Nelson-Overton LK, Siemsen DW, Gao Y, DeLeo FR, Quinn MT. Role of NF-kappaB in transcriptional regulation of the phagocyte NADPH oxidase by tumor necrosis factor-alpha. J Leukoc Biol 2007;82:729–741.
[55] Hidalgo C, Donoso P. Crosstalk between calcium and redox signaling: from molecular mechanisms to health implications. Antioxid Redox Signal 2008;10:1275–1312.
[56] Hidalgo C, Donoso P, Carrasco MA. The ryanodine receptors Ca2 + release channels: cellular redox sensors? IUBMB Life 2005;57:315–322.
[57] Zong H, Ward M, Stitt AW. AGEs, RAGE, and diabetic retinopathy. Curr Diab Rep 2011;11:244–252.
[58] Giacco F, Brownlee M. Oxidative stress and diabetic complications. Circ Res 2010;107:1058–1070.
[59] Barlovic DP, Soro-Paavonen A, Jandeleit-Dahm KA. RAGE biology, atherosclerosis and diabetes. Clin Sci (Lond) 2011;121:43–55.
[60] He CJ, Koschinsky T, Buenting C, Vlassara H. Presence of diabetic complications in type 1 diabetic patients correlates with low expression of mononuclear cell AGE-receptor-1 and elevated serum AGE. Mol Med 2001;7:159–168.
[61] Peter-Katalinic J, Fischer W. Alpha-d-glucopyranosyl-, d-alanyl- and l-lysylcardiolipin from gram-positive bacteria: analysis by fast atom bombardment mass spectrometry. J Lipid Res 1998;39:2286–2292.